AIAA 2002-0579
Wall-Pressure-Array Measurements Beneath a Separating / Reattaching Flow Region

Laura M. Hudy, Ahmed M. Naguib
Michigan State University
East Lansing, MI 48824

William M. Humphreys, Jr., Scott M. Bartram
NASA Langley Research Center
Hampton, VA 23681

40th Aerospace Sciences Meeting & Exhibit
14-17 January 2002 / Reno, NV

WALL-PRESSURE-ARRAY MEASUREMENTS BENEATH A SEPARATNG/REATTACHING FLOW REGION

Laura M. Hudy[*], Ahmed M. Naguib[†]
Michigan State University
East Lansing, MI 48823

William M. Humphreys Jr.[‡], Scott M. Bartram[§]
NASA Langley Research Center
Hampton, VA 23681

A database of wall-pressure array measurements was compiled for studying the space-time character of the surface-pressure field within a separating/reattaching flow region. The experimental setup consisted of a long splitter plate instrumented with an array of 80 flush-mounted microphones located within the wake of a fence. Data were acquired for a Reynolds number of 7885, based on the fence height. Two distinctive regions, defined based on their location relative to the position of the mean reattachment point (x_r) of the shear layer, emerged from this investigation. Upstream, from the fence to $\frac{1}{4}x_r$, the surface-pressure signature was dominated by large time scale disturbances and an upstream convecting velocity of $0.21U_\infty$. Beyond $\frac{1}{4}x_r$, turbulent structures with small time scales and a downstream convection velocity of $0.57U_\infty$ generated most of the pressure fluctuations. There was evidence that these structures began to form around $\frac{1}{4}x_r$ and grew in strength and size with downstream distance before reattaching on the plate. Only the time-averaged results from the microphones have been examined hitherto and will be presented.

Introduction

Separating/reattaching flows produce large pressure fluctuations on the underlying surface. These fluctuations could cause significant vibration of the surface and subsequent generation of noise. To predict and/o r control such vibration and noise effects one needs to understand the spatio-temporal character of the surface-pressure field. The present study addresses this issue through the use of a wall-microphone array to resolve the surface-pressure field both spatially and temporally in a basic separating/reattaching flow geometry. This provides further contribution to the bulk of the literature in this area, which has been primarily based on only one- or two-point measurements.

The flow geometry investigated in the current study consists of a splitter–plate attached to, and downstream of, a fence that is perpendicular to the flow, as shown in Figure 1. This model was used because it has a separation bubble that is elongated in the streamwise (x) direction, and hence the development of the wall-pressure field within the bubble can be resolved properly using a sensor array with inter-sensor spacing that is not too small to realize. Also in this geometry the boundary layer thickness is much smaller than the fence ('step') height, and therefore the boundary layer details have minimal affect on the flow field.
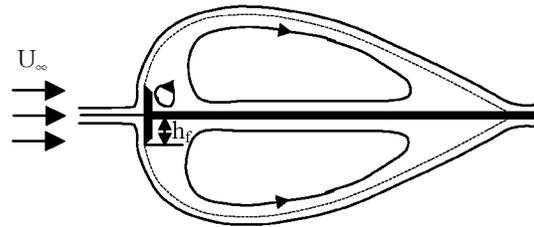

Figure 1. Splitter plate with fence flow geometry investigated and ideal two-dimensional flow field

Cherry *et al.*[1] made two-point unsteady surface pressure measurements in a separating/ reattaching flow region. Their test model geometry was a blunt-face splitter plate, which is similar in nature to the splitter-plate-with-fence geometry. The Reynolds number used in the experiment was based on the thickness of the

---

splitter plate and was held within the range of $3.2 \times 10^4 \pm 0.2 \times 10^2$. Cherry et al.[1] demonstrated the convective nature of the surface-pressure imprint associated with the downstream motion of the shear layer structures through cross-correlation analysis between two signals from microphones spaced apart in the streamwise direction. One microphone was fixed near the reattachment and the other was moved to five different positions from upstream to downstream of the fixed microphone. The peak in the cross-correlation function was seen to shift to a smaller time delay as the movable microphone was traversed in the downstream direction, indicating the convective nature of the flow structure dominating the wall-pressure generation process. Cherry et al.[1] also observed low- and high-frequency peaks in the power spectrum measured close to separation and near reattachment, respectively. They attributed the low-frequency signature to the flapping of the shear layer associated with the growth and decay of the separation bubble.

Farabee and Casarella[2] studied the fluctuating wall pressures in a forward- and backward-facing step flow using a flush-mounted B&K 1/8in. condenser microphone. Using frequency domain analysis, Farabee and Casarella[2] described the characteristics of the wall-pressure field as variable with x distance along the wall. Close to separation, the spectra showed the highest level of energy at low frequencies; whereas, farther downstream the spectrum containing the largest energy was found at reattachment. This was a manifestation of the increase in the energy of the organized, turbulent structures as the flow convected downstream. A corresponding shift was seen in the spectrum as the dominance of the low-frequency disturbances gave way to the dominance of the high-frequency structures downstream. A convection analysis at different positions along the model downstream of the step showed that the pressure fluctuations close to separation were associated with the re-circulating low-speed fluid and not the high-speed fluid in the shear layer. However, Farabee and Casarella[2] commented that the convection velocity was *always* in the downstream direction, indicating that the pressure fluctuations were not originating from the reverse flow within the re-circulating bubble.

Driver et al.[3], in their backward-facing step study of the time-dependent character of the separated shear layer at a Reynolds number of 37,000, based on the step height, noticed abnormal contraction and elongation of the separation bubble due to the shortening and lengthening of the reattachment length. This was labeled as the flapping motion of the shear layer with amplitude estimated to be 20% of the shear

layer width. They used surface pressure measurements along with velocity measurements to show that there was a definite low frequency disturbance associated with the shear layer flapping, but that it contributed very little energy to the overall pressure fluctuations.

Heenan and Morrison[4] investigated wall-pressure fluctuations behind a rearward-facing step and passive control of these fluctuations using a permeable surface (at Reynolds number equal to 1.9×10^5 based on the step height). Heenan and Morrison[4] found an upstream convection velocity close to separation using phase-angle analysis. They identified negative phase angles (with respect to a microphone signal measured immediately behind the step) at low frequencies and at locations from separation up to $0.4 x_r$ in the impermeable case. This is the only study found to date that describes an upstream convecting velocity.

Lee and Sung[5] used a 32-microphone array downstream of a backward-facing step to measure wall-pressure fluctuations in the streamwise and spanwise directions. Spatio-temporal statistics were completed on this comprehensive data set for a Reynolds number of 33,000, based on the step height. Lee and Sung[5] observed the same phenomenon in their experiment as experienced by earlier investigators of backward-facing-step studies. The RMS pressure fluctuations rose sharply starting around $0.5 x_r$ and peaked in the vicinity of reattachment, decaying beyond that point. Pressure spectra revealed low-frequency dominance close to separation, presumably due to the flapping of the shear layer. Farther downstream, the spectra were dominated by high-frequency components. In terms of convection velocity, Lee and Sung[5] calculated a downstream convection velocity of $0.6 U_\infty$ at high frequencies and they found no evidence of an upstream convection velocity. Although from their phase plot, (used to determine the convection velocity) there were many singularities (phase discontinuities) at low frequencies. This was not the case at the higher frequencies.

The characteristics described thus far in these surface pressure measurement studies have also been identified by authors that used different measurement techniques within similar type of geometries. In these separating/reattaching flow studies the measuring techniques used included hot-wire and pulsed-wire anemometry, skin-friction measurements, and particle image velocimetry. Castro and Haque[6], Eaton and Johnston[7], and Spazzini et al.[8] are a few of the authors who also observed very large-scale, low-frequency motion close to separation and small-scale, high frequency motion close to reattachment using these

techniques. In all studies, the low-frequency signature was attributed to the flapping of the shear layer.

Experimental Set-up

The present experiment was completed in the open-circuit, Subsonic Basic Research (Wind) Tunnel (SBRT) at NASA Langley Research Center in Hampton, Virginia. This low-speed wind tunnel has a 6:1 contraction section that measures 3.54 m in length. Located downstream of the contraction is a 0.57 m wide by 0.82 m high by 1.85 m long test section. Flow entering the wind tunnel is straightened using aluminum honeycomb flow straighteners and a double row of wire mesh turbulence screens. The fan is driven by a 200hp motor enabling flow speeds in the wind tunnel up to 60m/s. For this study, the flow speed (U_∞) used was 15m/s, resulting in a Reynolds number of 7885, based on the step height of the model. The corresponding turbulence intensity is less than 3%.

A schematic of the test model is shown in Figure 2, where x represents the streamwise distance measured from the fence, y is the normal distance from the splitter plate, z is the spanwise distance, h_f represents the step height above the splitter plate (8 mm), and 2H represents the total fence height (35 mm).
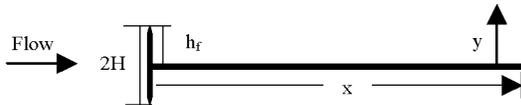
Flow → 2H h_f y x

Figure 2. Splitter-plate-with-fence configuration

The design of the model was symmetric with respect to top and bottom. It was constructed out of aluminum using a 12.7 mm thick aluminum skeleton support covered with 3.175 mm thick aluminum sheets, which provided storage space for the microphone wiring and static pressure tubing inside the model. The total length of the model was $160h_f$ or 73H and its width was $44h_f$ or 10H. Endplates were placed on the sides of the splitter plate to improve the two-dimensionality of the flow, according to Castro and Haque[6], resulting in a model aspect ratio of 36. The blockage ratio, as defined by Smits[9] who found that the reattachment distance decreased with increasing blockage ratio, was around 2%. This resulted in a reattachment length of approximately 0.2 m ($25.6h_f$), which ensured that the reattachment point would be contained within the extent of the microphone array.

The splitter plate was outfitted with 80 microphones and 80 static pressure taps. The configuration and numbering of the microphones and the static pressure taps are shown in Figure 3.

The microphone array consisted of Panasonic (WM-60A) omnidirectional back electret condenser microphone cartridges with a nominal sensitivity of -44±5 dB (relative to 1V/Pa) and a bandwidth of 20-20,000 Hz. The microphones, each with a sensing diameter of 2mm, were flush mounted and were used to record the fluctuating pressure on the surface of the plate. The center row consisted of 28 microphones spaced $1.2h_f$ apart center to center in the streamwise direction, starting at $0.6h_f$ downstream of the fence. On either side of the centerline, there were 2 rows each containing 13 microphones. These 13 microphones were spaced $2.4h_f$ apart center to center, except for three microphones in each row that were spaced $1.2h_f$ apart center to center. The spanwise spacing between the five rows was $6.4h_f$.
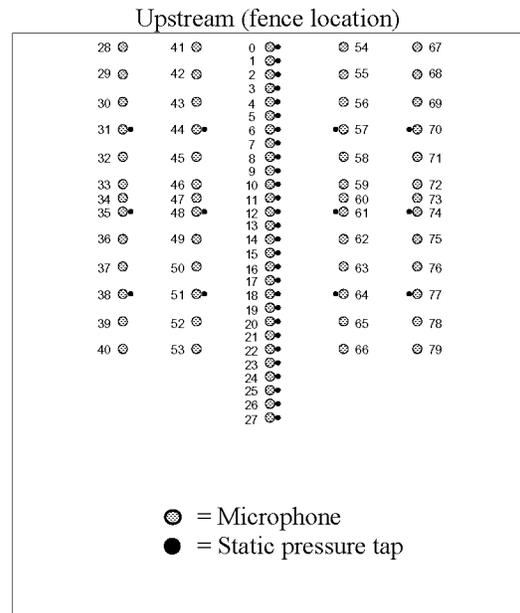
Upstream (fence location)

Figure 3. Top view of the instrument plate layout consisting of microphones and static pressure taps

Each microphone was calibrated against a ¼" B&K microphone with known sensitivity before being placed in the model. The outputs of sixty-four of the microphones were connected to eight National Instruments A/D Boards (SCXI 1141), placed in a SCXI 1001 chassis. Each board had an input signal range of ±5V, eight differential analog-input channels, and a variable channel gain that was set to one for this experiment. The highest sampling rate the board was capable of was 1.25 MHz for one channel. For the sixty-four channels, the corresponding maximum sampling rate was 19,531 Hz per channel resulting in an average time delay between successive channels of 2.6

μs. This delay, however, was small compared to a characteristic time scale of the flow convection over a distance equal to the microphone spacing: $\Delta/U_\infty = 635$ μs; where Δ is the spacing between successive microphones in the streamwise direction. Data for the experiment was sampled at 12kHz for 15 seconds, with the cut-off frequency anti-aliasing filters set at 5kHz.

The splitter plate was also instrumented with 40 static pressure taps on the top and bottom for a total of 80 taps. Static pressure measurements were primarily used to align the model in the tunnel and estimate the reattachment length. The location of the taps, which mirrored each other on top and bottom, is depicted in Figure 3. The static pressure taps were coupled to a 48-port Scanivalve that was connected to a Setra 239 series pressure transducer. The transducer measured differential pressure in the range of 0-25.4mm H_2O, outputting a corresponding 0-5V signal.
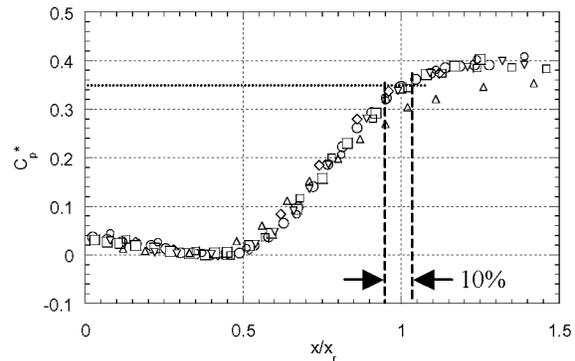
Results and Discussion

Reattachment length

The reattachment length (x_r) is an important parameter for the present flow geometry and, as shown by Ruderich and Fernholz[10], appears to be the appropriate length scale for this flow field. Therefore, before analyzing the data it was necessary to estimate the reattachment length for the purpose of normalizing the results. This was done utilizing the pressure coefficient (C_p^*) used by Ruderich and Fernholz[10] in their presentation of C_p results. The form for collapsing of C_p^* was first proposed by Roshko and Lau[11]. As Ruderich and Fernholz[10] explain, the mean pressure distribution results from different long-separation-bubble studies:

$$C_p^* = \frac{C_p - C_{p,min}}{1 - C_{p,min}} \qquad (1)$$

where C_p is defined as $(p_s-p_r)/(\frac{1}{2}\rho U_\infty^2)$, p_s is the surface pressure along the model, p_r is a reference pressure, measured with a static pressure tap located at the exit of the contraction, and $C_{p,min}$ is the minimum C_p in the mean pressure distribution. Figure 4 shows the C_p^* distribution for seven different studies, including the present one, as a function of the distance along the splitter plate normalized by the reattachment length. All seven studies, except Cherry et al.[1], used a splitter-plate-with-fence configuration. Cherry et al.[1] investigated a blunt-face splitter plate, with the thickness of the plate denoted by D. The legend displays details about each of the studies for which data are shown in Figure 4.

Although these studies were conducted at different Reynolds numbers and had various blockage ratios, resulting in a difference in the reattachment lengths, the pressure distribution for all experiments correlate well when plotted using the C_p^* coefficient, even in the case of the blunt-face-splitter-plate geometry. Thus, a universal pressure coefficient (C_p^*) value may be found at the mean reattachment location ($x/x_r = 1$), within the band of data scatter (about ± 5%). This value was determined to be approximately $C_p^* = 0.35$. By applying this C_p^* value to the present data, the reattachment distance could be determined within ± 5% uncertainty as shown in Figure 4. Therefore, the reattachment distance was determined to be roughly 205mm or 25.6h_f. Static pressure tap and microphone #21 is the port closest to this reattachment value and thus was used in the normalization of the present data throughout the study.

		Re	x_r/h_f or x/D	Blockage (%)
●	Present Measurements	0.8×10^4	25.6	1.94
◆	Castro & Haque (1987)	2.2×10^4	19.2	6.2
■	Cherry, Hillier & Latour (1984)	3.2×10^4	4.9	3.79
○	Ruderich & Fernholz (1986)	1.4×10^4	17.2	10
□	Ruderich & Fernholz (1986)	0.9×10^4	22.6	5.7
△	Roshko & Lau (1965)	1.4×10^4	33.6	5
▽	Hillier, Latour & Cherry (1983)	1.4×10^4	23.9	2.5

Figure 4. C_p^* distribution compared with six different studies

Mean and Fluctuating Pressure Distributions

Figure 5 shows the mean pressure distribution for three different studies, including the present measurements and data from Castro and Haque[6] and Cherry et al.[1], as a function of the distance along the instrument plate normalized by the reattachment

4
American Institute of Aeronautics and Astronautics

distance. There is good agreement between the current results and the Castro and Haque[6] data, which indicates the consistency of the mean-flow behavior around the constructed model with earlier studies of the same geometry. There is some offset between the present data and that from Cherry et al.[1] This offset could be due to the difference in model geometry. Comparison with Cherry et al.[1], however, was important because it was the only detailed study found with more than one-point unsteady surface pressure measurements in a separating/reattaching flow geometry similar in nature to the present experiment (i.e., one where the boundary layer thickness at separation is much smaller than the step height). Cherry et al.[1] conducted two-point measurements at different spacings on a splitter plate. Kiya and Sasaki[12] also studied the flow state over a blunt-face splitter plate using extensive single- and two-point measurements of surface-pressure and velocity measurements. However, they displayed most of their data in velocity and velocity-pressure correlation plots. It should also be noted that although the study of Lee and Sung[5], discussed in the Introduction, did utilize a 32-microphone array, their flow geometry was a backward facing step and not a splitter plate, with or without a fence.
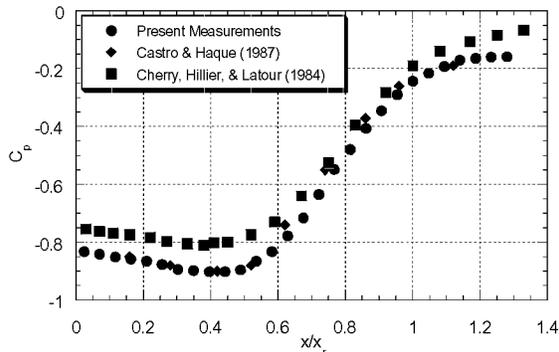

Figure 5. Streamwise distribution of the mean pressure coefficient for the current study compared to Castro and Haque[6] and Cherry et al.[1]

The root-mean-square (RMS) of the pressure fluctuation is shown in Figure 6 for the present study and that of Cherry et al.[1] The RMS data are plotted as $C_{p'} = p'_{rms}/\frac{1}{2}\rho U_\infty^2$ in Figure 6. The present data exhibit some scatter around the trend line, which is believed to be associated with the uncertainty of the microphone calibration procedure used to determine the sensitivities of the microphones. This uncertainty was found to be approximately 7%. There is qualitatively good agreement between the two data sets, although there is some difference as seen in the static pressure

measurements. This offset is largest in the vicinity of the peak in the $C_{p'}$ values and could be due to the difference in the model geometries selected for each study.

At the point of separation, the shear layer is laminar and relatively far away from the splitter plate wall-pressure sensors. At this location, the microphones detect low RMS pressure fluctuations directly behind the fence. It is unknown what causes these pressure fluctuations, but it has been theorized in the literature that the unsteadiness, or 'flapping', of the shear layer may in fact produce some of the wall-pressure activity seen in this region. The region referred to here is the distance from the fence up to about a quarter of the reattachment distance ($\frac{1}{4}x_r$), where the RMS values are relatively flat for both data sets shown in the graph. This region is significant and will be referred to in the upcoming sections.
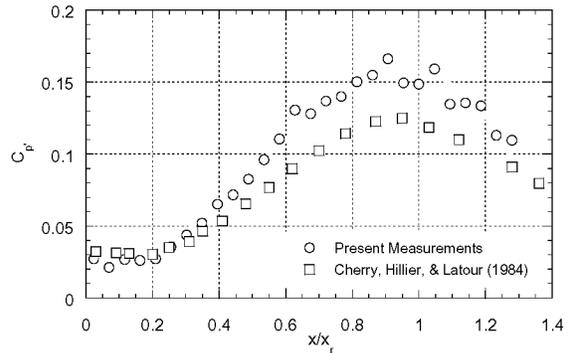

Figure 6. Streamwise distribution of the coefficient of RMS pressure fluctuations

Beyond the $\frac{1}{4}x_r$, there is a rise in the RMS pressure fluctuations, as seen in both data sets in Figure 6. It is believed that in this region the surface pressure fluctuations are predominately associated with the vortical structures of the separated shear-layer. As these structures convect downstream, growing in size and strength and moving closer to the wall, they produce an increasingly strong wall-pressure signature. The signature reaches a maximum level in the vicinity of where the flow impinges, or reattaches, on the plate as described by Farabee and Casarella[2]. It is well documented that the peak RMS value occurs slightly upstream of the reattachment point in both splitter-plate and backward-facing-step studies. Heenan and Morrison[4], in their backward-facing-step study, found the maximum RMS value to occur approximately one-step height upstream of reattachment. Beyond reattachment, the RMS values decrease slowly as the energized structures from the shear layer decay and

American Institute of Aeronautics and Astronautics

diffuse downstream. The flow then takes on boundary layer characteristics once the shear layer reattaches.

Auto-correlation and Integral Time Scales

To identify the dominant time scales in the measured wall-pressure time records, an auto-correlation analysis was conducted. The gray-scale contour map in Figure 7 shows the auto-correlation coefficient ($R_{p'p'}$) for all 28 centerline microphones. The abscissa shows the distance along the splitter plate with respect to the reattachment point, while the ordinate shows the time shift normalized by the free stream velocity and the total fence height. The color bar indicates the values of the auto-correlation coefficient, which was obtained by normalizing the correlation function by the square of the RMS of the signal. The map makes it easy to see the variation of the width of the auto-correlation with downstream distance and the transition between long and short timescales.
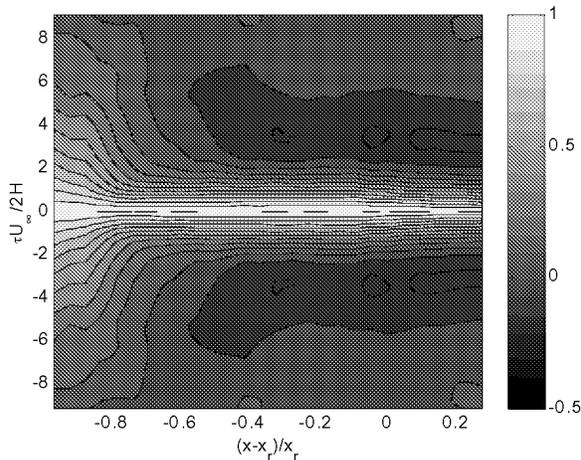

Figure 7. Contour map of the auto-correlation coefficient for all 28 microphones along the centerline of the model

In the region immediately behind the fence, the auto-correlation function extent is wide and changes very little up to a distance of about $0.2 - 0.25x_r$ ($x-x_r/x_r$ = -0.80 to –0.75) behind the fence. Farther downstream, this width narrows significantly over a relatively short distance (roughly from $0.25x_r$ to $0.7x_r$; $x-x_r/x_r$ = -0.75 to –0.30) as demonstrated by the focusing of the $R_{p'p'}$ contours towards $\tau U_\infty/2H = 0$ line. Beyond this region, the contour lines remain approximately parallel to the constant τ lines showing very little change in $R_{p'p'}$ with additional increase in x. The region between x/x_r = 0.25 to 0.7 roughly delineates the start and end locations of the change in

the time scales of the flow structures dominating $R_{p'p'}$. This region is referred to as the changeover region.

The dominance of low-frequency disturbances directly behind the fence has been identified in a number of studies. These include Castro and Haque[6], Cherry et al.[1], Driver et al.[3], Eaton and Johnston[7], Farabee and Casarella[2], and Lee and Sung[5]. Some of these studies have attributed these disturbances to the flapping of the shear layer as discussed in the introduction. Farther downstream, the organized shear layer structures grow in strength and move closer to the wall. These more energized structures impose a shorter time scale, than that encountered close to the fence, on the auto-correlation function. Thus, the increasing influence of these structures on the wall pressure appears to be responsible for the observed change in the $R_{p'p'}$ within the changeover region. Past this region, in the vicinity of the reattachment location and farther downstream, the energy of the shear layer organized structures appears to saturate (as seen in the RMS plot in Figure 6). This is possibly why no substantial change in $R_{p'p'}$ is detected past the changeover zone.

Figure 8 shows the streamwise variation of the integral time scale (τ^*) as a function of distance along the splitter plate with respect to the reattachment point. The integral time scale was derived from the auto-correlation function by finding the time at which the negative peak in the auto-correlation occurred with respect to the ordinate and multiplying that time value by two. Because of the even symmetry of the auto-correlation, τ^* gives the time delay between the two negative peaks in the auto-correlation function. An example of the method is shown in Figure 8a. The displayed error bars represent the uncertainty in locating the peak. A substantial error is encountered in the changeover region because the negative correlation peak in this region is flat, and therefore difficult to locate precisely in the presence of experimental data scatter (Figure 8b).

Figure 8 is similar in nature to that produced by Castro and Haque[6] using velocity measurements in the shear layer region. The results at the locations of the first four microphones show long time scales with relatively small error bars. This is the region closest to separation where other authors and this study have observed predominately low-frequency motion. Data from the next five microphones, associated with large error bars, are in the changeover area. The remaining microphones have shorter time scales with small error bars. This reaffirms the observations from the auto-correlation contour plot. That is, the signals from the microphones closest to separation are dominated by large time scales, whereas, the signals from the

6

microphones farther downstream are dominated by smaller time scales. In between, there is a changeover region starting roughly around ¼x_r, which is the same region seen in the RMS statistics. This region is believed to be associated with the amplification and streamwise development of the vortical shear layer structures.
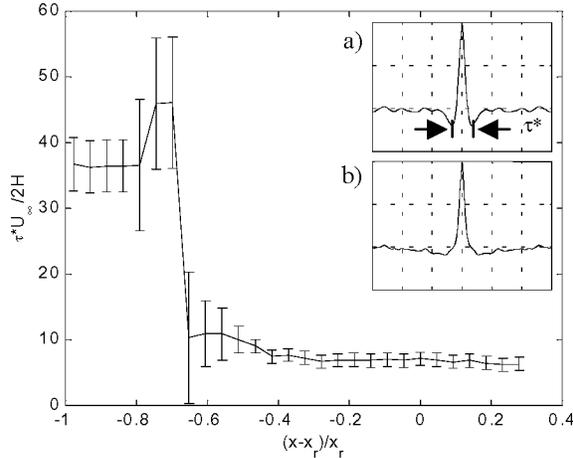

Figure 8. Streamwise variation of the integral time scale

Power Density Spectra

The power spectrum density at every third microphone along the centerline is shown in Figure 9. This figure contains the power spectrum plots on a logarithmic scale for both axes. The ordinate is plotted relative to an arbitrary reference value and represents the power spectrum normalized by the square of ½ρU_∞^2 and the abscissa represents the frequency normalized by the fence height and the free stream velocity. The use of the arbitrary reference value for the ordinate provides a means by which many spectrum plots can be shown on the same graph without clutter.

Figure 9 magnifies the spectra plots in order to get a closer look at the spectrum details and the shift in the peak frequency in the downstream direction. Close to separation, the peak in the frequency is seen to be roughly around $f(2H)/U_\infty$ = 0.02-0.03 (fx_r/U_∞ = 0.12-0.18) in the present study, which is the same peak seen by Cherry et al.[1]. In the case of the backward-facing step, Lee and Sung[5] also found a similar peak frequency value close to separation at fH/U_∞ = 0.015 (H = the height of the step), which when scaled by x_r instead gives a value of fx_r/U_∞ = 0.11. This is comparable to the values given by Spazzini et al.[8] at fx_r/U_∞ = 0.08 and Heenan and Morrison[4] at fx_r/U_∞ = 0.1. Cherry et al.[1] along with Heenan and Morrison[4], Driver et al.[3], and Lee and Sung[5], have associated this low-frequency peak

with the flapping of the shear layer. Farabee and Casarella[2] suggested that the energy distribution in the spectra indicates that the wall pressure fluctuations close to separation were caused by the unsteadiness of the low-speed re-circulating flow, rather than the highly turbulent structures in the shear layer. This is consistent with the fact that these structures are only beginning to develop in this region and are most likely weak compared to the strength of the low frequency disturbance produced by the shear layer movement.
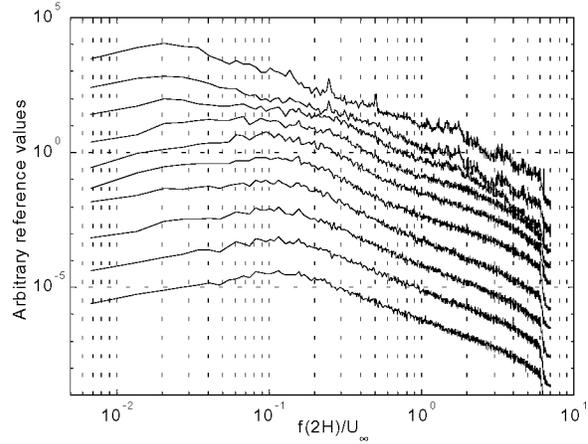

Figure 9. Power Spectra for selected microphones covering the measurement range - streamwise direction is from top to bottom

Farther downstream, the energy in the spectrum is located at higher frequencies as seen in the spectra in Figure 9. In particular, the peak in the spectrum occurs around $f(2H)/U_\infty$ = 0.1-0.15 (fx_r/U_∞ = 0.6-0.9), which is in agreement with the findings of Cherry et al.[1], where the frequency is normalized using the total width of the splitter plate in their case. Lee and Sung[5] stated that the power spectrum reaches a maximum at fH/U_∞ =0.068, or fx_r/U_∞ = 0.5. Spazzini et al.[8] found their maximum at fx_r/U_∞ = 1.0 along with Heenan and Morrison[4]. Driver et al.[3] recorded a peak value close to reattachment of fx_r/U_∞ = 0.6. This higher frequency peak has been attributed to the highly turbulent structures within the shear layer, as discussed previously.

Furthermore, it is interesting to compare the τ^* values obtained from the auto-correlation to the spectral peak frequencies. This comparison is possible because of the inverse relationship between time and frequency. For large time scales, the τ^* value close to the fence was determined to be $\tau^* U_\infty/(2H)$ = 36.5; thus the corresponding frequency is $f(2H)/U_\infty$ = 0.027, which is similar to the low-frequency peak found in the power spectra ($f(2H)/U_\infty$ = 0.02-0.03). Similarly, for the

7

smaller time scales farther downstream where the τ^* value is such that $\tau^*U_\infty/(2H) = 7.3$, resulting in a frequency of $f(2H)/U_\infty = 0.14$ compared to the $f(2H)/U_\infty = 0.1\text{-}0.15$ high-frequency peak from the power spectra. Castro and Haque[6] obtained velocity auto-correlation measurements at various positions in the shear layer using a pulsed-wire anemometer. From their results, they determined the time scale near separation to be 8 when normalized with the reattachment distance. This value compares well with $\tau^*U_\infty/x_r = 6.2$ calculated in the present study near the point of separation. The discrepancy could be due to the difference in the measuring techniques and/or the location where the data were recorded.

Cross-correlation with respect to measurements at reattachment

Figure 10 shows a gray-scale contour map (similar to Figure 7) of the cross-correlation coefficient of the signals from all 28 centerline microphones with that from the microphone closest to reattachment.
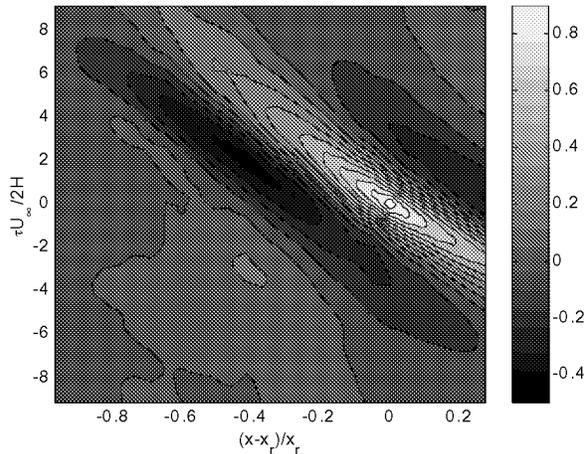

Figure 10. Cross-correlation-coefficient color contour map for all 28 centerline microphones (reference microphone closest to reattachment)

In the cross-correlation contour map, there is a main, positive correlation peak inclined at an angle and two negative lobes on either side of this main lobe. At each x location, the main peak is centered around time shift values corresponding to the largest positive correlation between the wall pressure signal at this x location and that at reattachment. The negative peaks give the time delay to the highest negative correlation. By finding the slope of the locus of the main positive (or negative) peak, an average downstream convective velocity can be calculated for the dominant turbulent structures regardless of their time scales (frequencies).

The velocity is calculated from the slope of the locus line using

$$\frac{1}{U_c} = \frac{m_s(2H)}{U_\infty x_r} \qquad (2)$$

where m_s is the slope of the locus line determined from a least-squares line fit and U_c is the convection velocity. Using equation (1), the convective velocity was determined to be 57% of the free stream velocity. Heenan and Morrison[4] reported, using two flush-mounted pressure transducers in their backward-facing-step configuration, convective velocities ranging between $0.5U_\infty$ and $0.6U_\infty$ depending on the position along the model. Lee and Sung[5] stated that convective velocities at high frequencies converged to a value of $0.6U_\infty$ in their backward-facing-step study, using a 32-microphone array. Hwang *et al.*[13] estimated the average convective velocity in their blunt-faced flat plate to be approximately $0.5U_\infty$ based on flow visualizations using a high-speed camera with high framing rates. Cherry *et al.*[1] determined the convective velocity to be $0.5U_\infty$ from pressure-pressure cross-correlations. Generally, the convective values were cited to range from 0.5 to 0.6 of the free stream velocity in the literature, depending on model geometry, location of measurement, and measuring technique. However, consideration of the results cited above suggests that the convective velocity values of the dominant structures in the splitter plate/fence flow are more similar to the backward-facing step, than to the blunt-facing plate.

Phase, Coherence, and more on Convection Speeds

The cross-correlation results yield an average convection velocity associated with various time scales. In order to determine the convection velocities associated with individual time scales (frequencies), the streamwise development of the phase angle (θ) was examined for various frequencies. θ at a given frequency and x location is computed from the cross spectrum between the microphone at that x location and the reference microphone (closest to the fence in the current results). However, before presenting the results for the phase plot, the range of frequencies for which reliable phase information can be calculated must be determined. This is accomplished by computing the coherence between the two signals for which the phase plot is to be obtained. The one-sided coherence between two signals obtained from N-point data records is defined as follows:

$$\Gamma_{p'_1 p'_2}(k) = \frac{\phi_{p'_1 p'_2}(k)}{\sqrt{\phi_{p'_1 p'_1}(k)\phi_{p'_2 p'_2}(k)}}; \quad (3)$$

$$k = 0,1,...\frac{N}{2}$$

where $\phi_{p'_1 p'_2}$ is the one-sided cross-spectrum between the two signals and $\phi_{p'_1 p'_1}$ and $\phi_{p'_2 p'_2}$ are the corresponding one-sided power spectra. The coherence gives a measure of the 'phase locking' between two signals at a particular frequency. If the signals are perfectly correlated across all frequencies, then the coherence value will be unity over the entire range. In general, a coherence value larger than 50% at a certain frequency is indicative of the existence of a fairly well defined phase between the two signals at that frequency. Thus, for frequencies where $\Gamma_{p'_1 p'_2} < 0.5$, the calculated phase values may not be reliable and will generally be randomly scattered. Figure 11 shows the coherence for neighboring microphones (numbering 0 and 1, 7 and 8, 16 and 17, and 26 and 27) to be high over a particular frequency range.
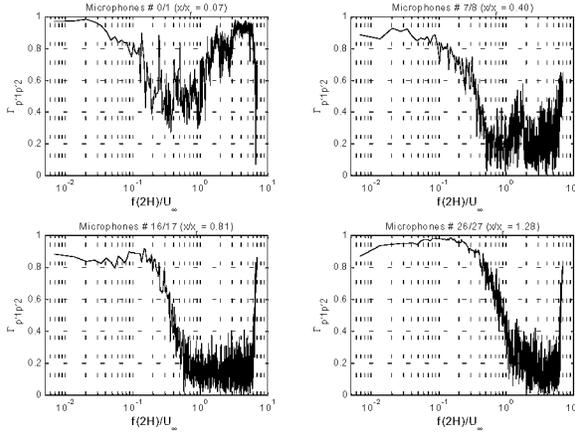

Figure 11. Coherence plot for four neighboring pairs of microphones

The coherence plots in Figure 11 reveal that the signals measured by adjacent pairs of microphones are not coherent (phase-locked) across all frequencies. In fact, there is a sharp drop off in the coherence around $f(2H)/U_\infty = 0.15$, immediately behind the fence. This value increases with x up to $f(2H)/U_\infty = 0.4$ at $x/x_r = 1.28$. This drop-off is seen in all four coherence plots, which provides a good representation of the high-coherence frequency range found for any two neighboring microphones along the centerline. Therefore, the phase analysis will be conducted using neighboring microphones and will be constrained to the

range up to $f(2H)/U_\infty = 0.3$ (this falls roughly in the middle of the range $f(2H)/U_\infty = 0.15$-0.4). It should be noted here that this frequency range contains the low- and high-frequency peaks identified earlier in the power spectrum behind the fence and farther downstream, respectively. Thus, all the flow structures of interest to the surface-pressure generation process are contained within the frequency range where high coherence is seen for two neighboring microphones.

Because of the use of pairs of neighboring microphones in calculating θ, there was no phase angle change greater than π between two signals at any frequency. This was confirmed by estimating a representative wavelength ($\lambda = U_c/f$) of the flow structures dominating the surface pressure measurements to be about $17h_f$, using the high-frequency peak $f(2H)/U_\infty = 0.15$ and the average convection velocity, $0.57U_\infty$. Since the space between neighboring microphones is $1.2h_f$, the phase angle difference between the two microphones would be, in the representative wavelength case, roughly 0.14π. Hence, there was no need to unwrap the angles.

Figure 12 displays a plot of the phase angle obtained using pairs of neighboring microphones as a function of the distance along the splitter plate for five different frequencies. By adding the phase angles from each of the pairs of microphones moving in the downstream direction, the phase shift relative to microphone #0 (closest to separation) was determined. The phase angles in the plot are calculated within the high-coherence frequency range. The distance along the splitter plate is referenced to the reattachment location.
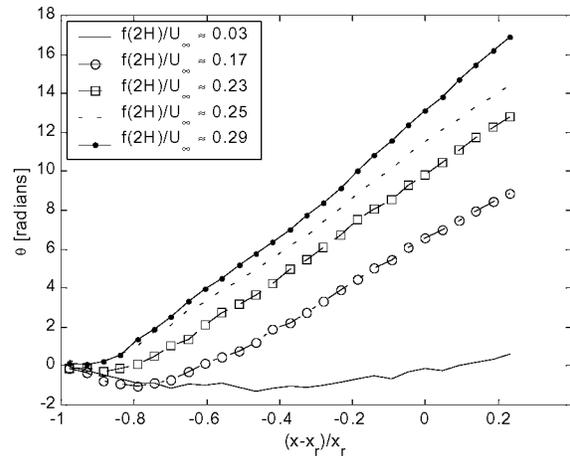

Figure 12. Streamwise development of the phase angle for five different frequencies (reference microphone at $(x - x_r)/x_r = -0.98$)

Except for the small region $(x-x_r)/x_r < -0.8$ in Figure 12, the phase plot reveals a steady, linear-like increase of the phase angle in the downstream direction for the four largest frequencies. The slopes of these lines differ, depending on the frequency. This indicates that there is a difference in the convective velocities corresponding to different frequencies. The convective velocity can be calculated by determining the slope of the phase plot line and using the following equation

$$U_c = \frac{2\pi f x_r}{\Delta\theta / \Delta x} \qquad (4)$$

where $\Delta\theta/\Delta x$ is the slope deduced from the phase plot using a least-squares line fit. A couple of points regarding this calculation should be noted here: (1) the line fit was restricted to about $(x-x_r)/x_r \geq -0.6$ where the phase characteristics behaved linearly, and (2) because the horizontal axis in Figure 12 is normalized by x_r, the calculated slope was divided by x_r to convert to physical units. The convection velocities for the different frequencies are given in Table 1. Averaging the five convection velocities give $0.64U_\infty$, which differs from the convection velocity $0.57U_\infty$ determined from the cross-correlation. This difference could be due to the fact that the velocities used in the average are not weighted by the relative dominance (energy) of the associated pressure fluctuations.

Table 1. Convective velocities for various frequencies

f(2H)/U∞	Uc/U∞
0.03	0.63
0.17	0.58
0.23	0.66
0.25	0.66
0.29	0.68

At $f(2H)/U_\infty = 0.17$ in Figure 12, the phase drops below zero. This is indicative of an upstream convecting velocity. Heenan and Morrison[4] is the only other investigation reporting negative phase angles, in their study of a backward-facing step. Lee and Sung[5] mention the idea of an upstream convecting velocity but found no evidence of this phenomenon in their study. The largest negative phase angle at $f(2H)/U_\infty = 0.17$ is found around microphone #4. After further investigation at various frequencies (ranging from $f(2H)/U_\infty = 0.07$ to $f(2H)/U_\infty = 0.22$), it was seen that the largest negative peak fluctuated between microphones #4, 5, and 6. These microphones are

roughly around a ¼ of the way to reattachment. Interestingly, this region was also identified earlier in both the RMS and the auto-correlation results, upstream of the changeover region.

In the case of $f(2H)/U_\infty = 0.03$, which corresponds to the low-frequency peak identified in the power spectra, the phase angle drops below zero but has a maximum negative peak farther downstream of microphones #4, 5 and 6. The peak is located near microphone #11. This indicates that the upstream convection velocity seen in the region spanning from the fence to microphone #4 at frequency $f(2H)/U_\infty = 0.17$ extends farther downstream to microphone #11 at frequency $f(2H)/U_\infty = 0.03$. Therefore, flow structures at very low frequencies can be seen, as evidenced by the phase plot, convecting upstream starting from a distance $x/x_r = 0.53$ downstream of separation. It is not clear if this could be associated with the flapping of the shear layer, which has been hypothesized to correspond to the low-frequency peak in the spectrum by various authors including Castro and Haque[6].

To explore the convective characteristics of the surface pressure around $x/x_r = ¼$ further, the cross-correlation function for all 28 microphones relative to the middle microphone #5 (which is located at about $x/x_r = 0.26$) was calculated and plotted in Figure 13.
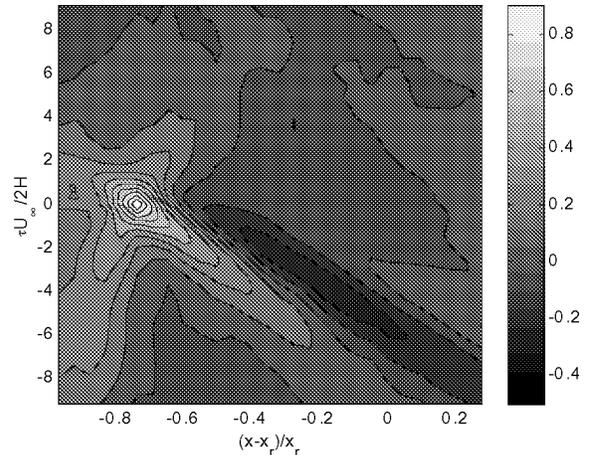

Figure 13. Cross-correlation-coefficient contour plot for all 28 (reference microphone at $(x-x_r)/x_r = -0.74$)

From the contour plot, an inclined positive peak is found on either side of the high correlation coefficient peak at microphone #5. These two peaks have opposite signed slopes with respect to each other. This is evidence that there are two convecting velocities: one upstream and one downstream as also deduced by Heenan and Morrison[4] from phase measurements. The present study is the first to depict

American Institute of Aeronautics and Astronautics

the upstream convection from the space-time correlation function. Additionally, the evidence of downstream-traveling motion in Figure 13 shows that the flow structures dominant farther downstream from microphone #5 (those corresponding to the power spectrum peak at $f(2H)/U_\infty = 0.1\text{-}0.15$) are detectable as early as microphone #5. To check for the earliest manifestation of the downstream convecting motion, the cross-correlation map is obtained for all 28 microphones relative to microphone #0 as shown in Figure 14. The axes are the same as in Figure 13.

The cross-correlation results in Figure 14 reveal that the downstream convecting velocity begins roughly around the $\frac{1}{4}x_r$ distance, as evidenced by the negative-inclined contour that starts at this position. Upstream of $\frac{1}{4}x_r$, there are no negative-inclined lobes indicating a downstream convecting velocity. Therefore, it is reasoned that the flow structures seen to dominate the measurements downstream are first noticeable in the surface pressure measurements around the $\frac{1}{4}x_r$ distance.
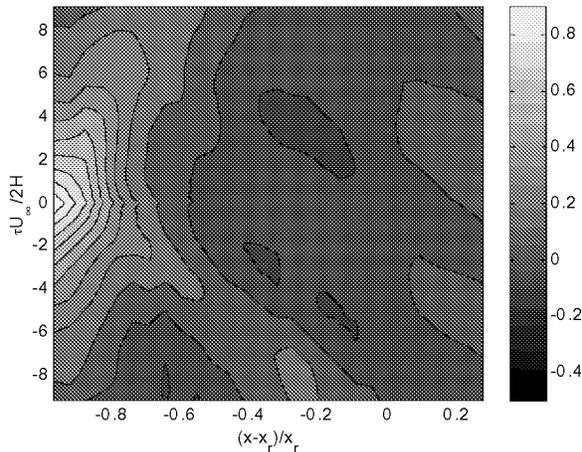

Figure 14. Cross-correlation-coefficient contour plot for all 28 (reference microphone at $(x-x_r)/x_r = -0.98$)

The upstream convecting velocity was determined to be 21% of the free stream velocity. This is similar to the value determined by Heenan and Morrison[4]. Their value was about 20% of the free stream velocity. The downstream convecting velocity was calculated to be 47% of U_∞. This value is lower than 57% U_∞ calculated earlier from the cross-correlation map with the reference microphone located closest to reattachment (Figure 10). Heenan and Morrison[4] also noticed this trend in their impermeable backward-facing step. Upstream near the fence, they observed a $0.5U_\infty$ convecting velocity that increased to

$0.6U_\infty$ close to reattachment and continued to rise farther downstream.

Concluding Remarks

The space-time characteristics of the surface-pressure within the separating/reattaching flow region of a splitter-plate-with-fence configuration were studied. For this purpose, a comprehensive database was compiled using an 80-microphone array embedded in the wall of the splitter plate. Only the time-averaged space-time statistics of the surface pressure measurements have been presented in this paper. In general, the results from this analysis compared well with available literature in related, but not exactly similar flow geometries.

The streamwise distribution of RMS pressure fluctuations exhibited a rapid rise in magnitude around $\frac{1}{4}x_r$, with the peak value occurring in the vicinity of reattachment. The region extending up to $\frac{1}{4}x_r$ was also identified in the auto-correlation function analysis, which showed decreasing time scales with downstream distance. The $R_{p'p'}$ contour plot revealed that within the $\frac{1}{4}x_r$ region the surface-pressure signature was dominated by large time scales. Farther downstream, near reattachment, smaller time scales were prominent in the wall-pressure measurements. Transition between the two different time scales occurred in a region extending from $0.25x_r$ to $0.7x_r$.

The peak energy in the power spectra for microphones close to the fence is concentrated at very low-frequencies ($f(2H)/U_\infty = 0.02 - 0.03$), which has been attributed by many researchers to the 'flapping' of the shear layer. Farther downstream near the mean reattachment location, the concentration of peak energy in the power spectra is seen at a higher frequency ($f(2H)/U_\infty = 0.1\text{-}0.15$), relating to the highly turbulent structures within the shear layer. The findings from the auto-correlation function and power spectra analyses were consistent.

From the cross-correlation function analysis, with respect to a reference microphone located closest to reattachment, the wall-pressure signature of the downstream convective motion of shear-layer structures, described by Cherry et al.[1] amongst others, was found to travel at a convection velocity of $0.57U_\infty$. Phase angle information, obtained from the cross-spectrum of the signal between neighboring pairs of microphones and constrained to frequencies up to $f(2H)/U_\infty = 0.3$ (range of high signal coherence), revealed an upstream convecting velocity of $0.21U_\infty$ at low frequencies within the $\frac{1}{4}x_r$ region. A cross-correlation contour plot, based on a reference microphone located near $\frac{1}{4}x_r$, showed the two opposing

convection velocities and provided evidence that the earliest detection of the downstream-traveling turbulent structures seen near mean reattachment was around $\frac{1}{4}x_r$.

Overall, two distinctive regions emerged from the spatio-temporal analysis of the surface pressure measurements in both the time and frequency domains. Upstream, from the fence to $\frac{1}{4}x_r$, the surface-pressure signature was dominated by large time scale disturbances and an *upstream* convecting velocity of $0.21U_\infty$. Beyond the $\frac{1}{4}x_r$, turbulent structures with small time scales and a downstream convection velocity of $0.57U_\infty$ generated most of the pressure fluctuations.

[1] **Cherry NJ; Hillier R; Latour MEMP** (1984) Unsteady measurements in a separated and reattaching flow. J Fluid Mech 144: 13-46

[2] **Farabee TM; Casarella MJ** (1986) Measurements of fluctuating wall pressure for separated/reattached boundary layer flows. J of Vibration, Acoustics, Stress, and Reliability in Design 108: 301-307

[3] **Driver DM; Seegmiller HL; Marvin JG** (1987) Time-dependent behavior of reattaching shear layer. AIAA J 25: 914-919

[4] **Heenan AF; Morrison JF** (1998) Passive control of pressure fluctuations generated by separated flow. AIAA J 36: 1014-1022

[5] **Lee I; Sung HJ** (1998) Characteristics of wall pressure fluctuations in separated and reattaching flows over a backward-facing step: Part I. Time-mean statistics and cross-spectral analyses. Experiments in Fluids 30: 262-272

[6] **Castro IP; Haque A** (1987) The structure of a turbulent shear layer bounding a separation region. J. Fluid Mech 179: 439-468

[7] **Eaton JK; Johnston JP** (1981) A review of research on subsonic turbulent flow reattachment. AIAA J 19: 1093-1100

[8] **Spazzini PG; Iuso G; Onorato M; Zurlo N; Di Cicca GM** (2001) Unsteady behavior of back-facing step flow. Experiments in Fluids 30: 551-561

[9] **Smits AJ** (1982) Scaling parameters for a time-averaged separation bubble. AIAA J 104: 178-184

[10] **Ruderich R; Fernholz HH** (1986) An experimental investigation of a turbulent shear flow with separation, reverse flow, and reattachment. J Fluid Mech 163: 283-322

[11] **Roshko A; Lau JC** (1965) Some observations on transition and reattachment of a free shear layer in incompressible flow. In Proc. 1965 Heat Transfer and Fluid Mech. Inst.

[12] **Kiya M; Sasaki K** (1983) Structure of a turbulent separation bubble. J Fluid Mech 137: 83-113

[13] **Hwang KS; Sung HJ; Hyun JM** (2000) Visualizations of large-scale vortices in flow about a blunt-faced flat plate. Experiments in Fluids 29: 198-201